Dynamics of Atmospheres and Oceans, 7 (1983) 233–263
Elsevier Science Publishers B.V., Amsterdam – Printed in The Netherlands

THE PHYSICAL SIGNIFICANCE OF MODONS: LABORATORY EXPERIMENTS AND GENERAL INTEGRAL CONSTRAINTS

GLENN R. FLIERL [1], MELVIN E. STERN [2] and JOHN A. WHITEHEAD, Jr. [3]

[1] *Massachusetts Institute of Technology, Cambridge, MA 02139 (U.S.A.)*
[2] *University of Rhode Island, Kingston, RI 02881 (U.S.A.)*
[3] *Woods Hole Oceanographic Institution, Woods Hole, MA 02543 (U.S.A.)*

(Received October 8, 1982; revised April 28, 1983; accepted May 9, 1983)

ABSTRACT

Flierl, G.R., Stern, M.E. and Whitehead, Jr., J.A., 1983. The physical significance of modons: laboratory experiments and general integral constraints. Dyn. Atmos. Oceans, 7: 233–264.

A barotropic jet emerging from a point source in a rotating fluid is deflected to the right (northern hemisphere) and starts to accumulate in an anticyclonic vortex. This gives rise to a cyclonic neighbor, and the dipole (modon) then propagates away from the source in a circular path. A modification of Batchelor's (1967) solution, which takes into account the different strengths of the anticyclonic–cyclonic pair, is able to account for the path curvature. The experiment shows that highly organized modons can be realized in the laboratory with rather nondescript forcing. The β-effect (not noticeably present in the experiment) should enhance the realizability of these structures in geophysical flows. Therefore, it is suggested that the modon model captures certain essential features of geophysical eddies. This is based on a derived theorem which shows that any *slowly varying* (not necessarily uniformly propagating) and *isolated* disturbance on the beta plane must have zero net relative angular momentum, so that the dipole is the simplest dynamically consistent representation of such a disturbance. Some interesting aspects of two-dimensional turbulence in a rotating fluid are also indicated by the laboratory experiments and by the general integral theorems presented.

1. INTRODUCTION

In the mid-latitude atmosphere and oceans, synoptic-scale disturbances dominate the flow patterns, and through their transports of heat, vorticity or momentum, regulate the general circulation. While many of these flows appear random to some degree, there are also striking examples of coherent and apparently isolated features which seem relatively stable to the fluctuations occurring around them. Atmospheric blocks, while showing somewhat of a "wake" structure are not strongly correlated with the motions around the globe (Dole, 1982). Hurricanes and other severe weather systems seem

0377-0265/83/$03.00

even more independent of nearby fluctuations. In the oceans, current rings (cf. The Ring Group, 1981) and small-scale strong eddies (McWilliams et al., 1983) are oft-quoted prototypes of isolated features. Finally, of course, there is the most colorful example of an independent eddy—the Great Red Spot of Jupiter, a vortex which has existed in a region of strong shears and fluctuations for over 300 years.

The study of isolated synoptic-scale structures such as is undertaken here, may also be useful in constructing a hierarchy of models applicable to the "great outdoors". The results of surface gravity wave dynamical studies, for example, indicate that solitons are the basic building blocks from which more complex patterns are constructed. Perhaps a similarly useful decomposition could be found for the oceanic or atmospheric synoptic eddy field.

The search for consistent isolated solitons has led to the discovery of a set of strongly non-linear solutions on the beta plane. All of these are form-preserving solutions and all have a multiple vortex structure (Stern, 1975; Larichev and Reznik, 1976a, 1976b; Flierl et al., 1980), with zero net relative angular momentum. In this paper, we will relax the condition that the disturbance be steadily moving, and we shall show that any isolated, slowly evolving disturbance in a stratified fluid (with arbitrary background flows) on the beta plane must have no net relative angular momentum.

The qualifying terms "isolated" and "slowly varying" are important caveats which we shall define more fully below. However, they are not at all inconsistent with our usual conceptions of synoptic-scale dynamics. The basic result of our analysis is

$$\beta \iint \mathrm{d}x\mathrm{d}y\, \psi(x, y, t) = 0$$

where ψ is the streamfunction for the depth-averaged flow and β is the northward gradient of the Coriolis parameter. This applies to isolated eddies (in the absence of topography, cf. Rizzoli and Hendershott, 1980), whether or not the motion is steady or evolving; whether or not the fluid around the eddy is at rest or moving with horizontal or vertical shears. This condition on ψ is equivalent to requiring that the net relative angular momentum of the eddy must be zero.

The simplest structure satisfying this requirement is the modon. The theorem suggests that, on the beta plane, such features may be dynamically natural and significant, particularly in the barotropic flow field. Likewise, modons may also be important in determining the distributions of many properties, such as salinity in the ocean, since they are capable of transporting material large distances from the formation region. However, there is some question about the conditions under which highly organized dipole structures can arise. We feel that some illumination has been cast upon this

question both by the theoretical studies of Frederiksen (1982) and Baines (1983), and perhaps even more convincingly by the laboratory experiments of Griffiths and Linden (1981), where modons can be seen quite distinctly. Here, we shall describe some even simpler laboratory experiments in which modon structures are generated by rather nondescript forcing—strong jet-like intrusions into a rotating fluid. Modons are formed as the jet is deflected azimuthally, and a large fraction of the radially outward transport of the entering fluid is accomplished by dipole formation and the propagation of these structures through the surrounding water. To a first approximation, these eddies are modeled as a Batchelor (1967) dipole, the main difference being that the center of the experimental dipole moves in a curved path. This behavior will be accounted for by a modification of Batchelor's solution. We emphasize that the vanishing of the angular momentum can be achieved with patterns other than a *simple* dipole; in particular, the compensating counter-rotating flows could occur at depth (for baroclinic motions) or around the outside of an eddy.

2. ZERO NET ANGULAR MOMENTUM—A THEOREM

There are many possible derivations of this basic theorem, depending on the particular equations chosen as a starting point. We shall state here the most general case of interest to atmospheric and oceanic dynamicists. Consider a fluid satisfying the "anelastic" equations (Batchelor, 1953; Ogura and Phillips, 1962) in which the density term in the horizontal momentum and the mass equations is replaced by a hydrostatically balanced density, $\rho_s(z)$. This approximation filters out the sound waves. We need consider only the northward (y) momentum equation

$$\frac{\partial}{\partial t}\rho_s v + \nabla \cdot (\mathbf{v}\,\rho_s v) + f u \rho_s = -\frac{\partial}{\partial y}p - \frac{\partial}{\partial x}\tau_{xy} - \frac{\partial}{\partial y}\tau_{yy} - \frac{\partial}{\partial z}\tau_{zy}$$

and the mass conservation equation

$$\nabla \cdot (\mathbf{v}\,\rho_s) = 0$$

where $f(y)$ is the Coriolis parameter, (u, v, w) are the (x, y, z) components of the total relative velocity, $\mathbf{v}$, p is the normalized pressure and the (turbulent) stresses are denoted by τ.

The motion will be divided into two parts, one of which is a background flow denoted by $\bar{\mathbf{v}}$, $\bar{p}$ and $\bar{\tau}$, satisfying the above equation by itself. A simple example would be a laminar zonal flow varying with latitude and depth. The second component is a superimposed isolated eddy field, $\mathbf{v}'$, p' and τ'. When the equations for $\bar{\mathbf{v}}$, $\bar{p}$ and $\bar{\tau}$ are subtracted from the equations above, we get

$$\frac{\partial}{\partial t}\rho_s v' + \nabla \cdot \left[\bar{\mathbf{v}}\,\rho_s v' + \mathbf{v}'\,\rho_s \bar{v} + \mathbf{v}'\,\rho_s v'\right] + f\,\rho_s u'$$

$$= -\frac{\partial}{\partial y}p' - \frac{\partial}{\partial x}\tau'_{xy} - \frac{\partial}{\partial y}\tau'_{yy} - \frac{\partial}{\partial z}\tau'_{zy}$$

$$\nabla \cdot (\rho_s \mathbf{v}') = 0$$

Note that no linearization or small amplitude assumption has been made here. Furthermore, the background field ($\bar{\mathbf{v}}$, $\bar{p}$ and $\bar{\tau}$) need not be zonally symmetric (or even steady). The formalism can be applied to as diverse phenomena as the motion of a Gulf Stream ring in the ocean or the motion of the Red Spot in the highly sheared flow on Jupiter. In either case, the natural assumption is that these features are isolated spatially so that they could be understood by a model with ($\mathbf{v}'$, p') going to zero far from the center. We shall vertically integrate both of these equations, applying the boundary condition

$$\rho_s w' = 0$$

at the top and bottom of the domain. These conditions restrict us to flat-bottomed geometries and also filter out external gravity waves. In addition, the restrictive upper boundary conditions alter the form of very long barotropic Rossby waves in ways which will be discussed more thoroughly below.

The integrated mass conservation equation states that the horizontal mass transport is nondivergent, and therefore a streamfunction $\psi(x, y, t)$ can be defined by

$$\int \mathrm{d}z \rho_s u' = -\psi_y, \qquad \int \mathrm{d}z \rho_s v' = \psi_x$$

From these definitions, it follows immediately that the net linear momenta in the horizontal directions will vanish

$$\iint \mathrm{d}x\mathrm{d}y \int \mathrm{d}z \rho_s u' = 0, \qquad \iint \mathrm{d}x\mathrm{d}y \int \mathrm{d}z \rho_s v' = 0$$

as long as the streamfunction vanishes faster than $1/r$ far from the eddy. This is one of the restrictions which will specify precisely what we mean by "isolated".

The integral of the momentum equation over all three dimensions is

$$\frac{\partial}{\partial t}\iint \mathrm{d}x\mathrm{d}y \int \mathrm{d}z \rho_s v' + \oint \mathrm{d}l \int \mathrm{d}z \left[(\hat{\mathbf{n}} \cdot \bar{\mathbf{v}})\, v' + (\hat{\mathbf{n}} \cdot \mathbf{v}')\, \bar{v} + (\hat{\mathbf{n}} \cdot \mathbf{v}')\, v'\right] \rho_s$$

$$+ \iint \mathrm{d}x\mathrm{d}y \int \mathrm{d}z \rho_s u' = -\oint \mathrm{d}l \int \mathrm{d}z p' \hat{y} \cdot \hat{\mathbf{n}} - \oint \mathrm{d}l \int \mathrm{d}z \hat{\mathbf{n}}_i \tau'_{iy}$$

$$- \iint \mathrm{d}x\mathrm{d}y \tau'_{zy}(\text{top}) + \iint \mathrm{d}x\mathrm{d}y \tau'_{zy}(\text{bottom})$$

where the line integral (dl) is over a curve at large radial distances from the isolated eddy, and $\hat{\mathbf{n}}$ is a unit vector normal to this curve. The momentum advection terms vanish, provided $\mathbf{v}' \to 0$, faster than $1/r$, which is certainly consistent with the requirement placed on the barotropic component ($\psi = o(1/r)$) and which places a similar restriction on the baroclinic component. The term involving the stress at the lateral boundary will also vanish. The key term is the one with the time derivative which vanishes according to the previous kinematical result that the net linear momentum vanishes at all times. This is the content of the "slowly varying" restriction: not only is ψ required to be $o(1/r)$ initially, but also ψ_t is required to be $o(1/r)$ so that the integral of the time derivative terms vanishes. Finally, we assume p' decays as $o(1/r)$, which is consistent with a dominant geostrophic balance in the far field of the eddy. Thus we see that the only non-vanishing terms in the y-momentum equation are the Coriolis term and the bottom/top viscous stress. Since f equals a constant plus βy, we have

$$\beta \iint dx\,dy\, y \int dz\, \rho_s u' = -\left[\iint dx\,dy\, \tau_{zy} \right]_{\text{bottom}}^{\text{top}}$$

Under typical modeling assumptions for evolution of oceanic mesoscale or atmospheric synoptic-scale motions, the right-hand side will vanish. Often, these stresses are dropped completely, and at most a horizontal stress term is included (e.g., layer models or inviscid models). However, we can also show that the contribution of the right-hand side vanishes when the bottom friction is obtained using the well-known Ekman layer parameterization, whereby the stress is proportional to a linear combination of the geostrophic velocities directly above the viscous boundary layer. Since these velocities are in turn proportional to the horizontal pressure derivatives, the horizontal integrals of the bottom stress will vanish for our isolated solutions, and thus we concluded that

$$\beta \iint dx\,dy\, y \int dz\, \rho_s u' = 0$$

to a very good approximation. This is equivalent to

$$\beta \iint \psi\, dx\,dy = 0$$

provided we use a somewhat stronger condition on the behavior of the stream function at infinity, viz. $\psi = o(1/r^2)$. Alternatively, we can use the net relative angular momentum

$$M = \iint dx\,dy \int dz\, \rho_s (xv' - yu') = -2 \iint dx\,dy\, \psi$$

and conclude

$$M = 0$$

if $\psi \to 0$ faster than $1/r^2$. This conclusion is a generalization of the results obtained previously for uniformly propagating eddies, and the most important assumption is $\psi = o(1/r^2)$ as $r \to \infty$.

If the latter condition is satisfied, a monopole on the beta plane is impossible because the net Coriolis force in the north–south direction would be non-zero, and there is no other force which can compensate for the imbalance. The dipole modon solutions and the approximate solutions discussed by Larichev and Reznik (1976b) clearly satisfy the integral constraint. For other cases, the proof is more difficult, but can still be obtained: for the barotropic solitary wave in a shear flow discussed (for application to the Red Spot) by Maxworthy and Redekopp (1976), the cross-stream structure $\phi(y)$ is set by the solutions of the stability equation for long disturbances,

$$(U-c)\frac{\partial^2}{\partial y^2}\phi + \left[\beta - \frac{\partial^2}{\partial y^2}(U-c)\right]\phi = 0$$

This can be integrated to show that $\beta \int \mathrm{d}\, y\phi = 0$ as long as the eddy is isolated (not reaching to the north-south edges of the domain). The barotropic solutions, therefore, do not seem to be appropriate for representing the Red Spot, and these authors go on to describe a baroclinic solution. For the stratified case (and also for the stratified eddy models of Redekopp (1977) or Flierl (1979), the eddy has a baroclinic mode vertical structure so that although there is net relative angular momentum in the upper levels, there is opposite flow in the deep fluid with precisely canceling angular momentum. The model of Ingersoll and Cuong (1981) did not explicitly consider the deep flow field; however, if this field is also isolated, it must have opposite circulation to the upper level flow. All these theoretical considerations seem to imply the existence of an "antispot" deeper within Jupiter's atmosphere. Finally, the barotropic "rider" solutions of Flierl et al. (1980) also have angular momentum in the exterior which cancels that in the interior.

The clearest motivation for adopting the isolation concept comes from the observation of ocean eddies, many of which have water mass characteristics distinctly different from their surroundings. Moreover, the observer is frequently compelled (for obvious reasons of data limitation) to *implicitly* regard his eddy as self-contained, due regard being made for an occasional jostle by a neighboring eddy or a slow drift associated with the mean circulation. Likewise, one approach to modeling such structures is to minimize far field eddy motions.

3. THE ADJUSTMENT PROCESS

Despite these remarks which indicate the restrictions on the use of our general theorem, there is a paradoxical element to it which must be resolved. Surely one can conceive of an initial state on the beta plane having non-zero angular momentum (a monopole) and the question is how such a state can be reconciled with our theorem.

The answer seems to be that an initially isolated eddy with non-zero net angular momentum must have a tendency field which is *not* isolated so that there will be finite boundary integrals which balance the non-zero Rossby vortex force. The signals necessary to set up these flows at the boundaries can be carried by acoustic, gravity or Rossby waves, and we now argue that the latter—(long barotropic) Rossby waves—are the most important mechanisms in the monopole adjustment problem.

First, we note the key role played by the β-effect in the proof of the theorem. Without the variations of f, the net Coriolis force on a monopole would vanish, and the momentum equation would be balanced identically.

Second, we can consider the case of the barotropic flow

$$\frac{\partial}{\partial t}\nabla^2\psi + J(\psi, \nabla^2\psi + \beta y) = 0$$

where only Rossby waves can exist. If we multiply this equation by x and integrate horizontally, we find

$$\oint \mathrm{d}l\, \nabla\psi_t \cdot \hat{\mathbf{n}} x - \oint \mathrm{d}l\, \hat{\mathbf{x}} \cdot \hat{\mathbf{n}}\psi_t + \oint \mathrm{d}l\, \psi \hat{\mathbf{k}} \cdot [\hat{\mathbf{n}} \times \nabla(\nabla^2\psi + \beta y)]x$$

$$- \oint \mathrm{d}l\, \psi \nabla\psi_y \cdot \hat{\mathbf{n}} + \oint \mathrm{d}l\, \hat{\mathbf{y}} \cdot \hat{\mathbf{n}} \frac{|\nabla\psi|^2}{2} = \beta \iint \mathrm{d}x\mathrm{d}y\psi$$

For an eddy isolated at all times, the boundary integrals must vanish, implying that $\iint\psi = 0$, as before. But if the latter condition is not satisfied in the initial state, then we shall show that the tendency field, ψ_t, will not be isolated; and will yield finite boundary terms, so that the first two integrals above will not vanish.

This can be demonstrated easily from the integral form of the equation for the tendency, ψ_t

$$\psi_t(\mathbf{r}') = -\frac{1}{2\pi}\iint \mathrm{d}x\mathrm{d}y \ln|\mathbf{r}' - \mathbf{r}|[\beta\psi_x + J(\psi, \nabla^2\psi)]$$

If we evaluate ψ_t as $r' \to \infty$ by expanding in r/r', we find

$$\psi_t(\mathbf{r}') \simeq -\frac{\ln r'}{2\pi}\iint \mathrm{d}x\mathrm{d}y G(\mathbf{r}) - \frac{\cos\theta'}{2\pi r'}\iint \mathrm{d}x\mathrm{d}y\, xG - \frac{\sin\theta'}{2\pi r'}\iint \mathrm{d}x\mathrm{d}y\, yG +$$

$$+\frac{1}{4\pi r'^2}\left[\cos 2\theta' \iint \mathrm{d}x\mathrm{d}y(x^2-y^2)G - \sin 2\theta' \iint \mathrm{d}x\mathrm{d}y xyG\right] + \ldots$$

where $G = \beta\psi_x + J(\psi, \nabla^2\psi)$. For an isolated *initial* field, we can evaluate the integrals above by partial integrations to derive

$$\psi_t(\mathbf{r}') \simeq \frac{\beta\cos\theta}{2\pi r'} \iint \psi \mathrm{d}x\mathrm{d}y - \frac{2\beta\cos 2\theta'}{4\pi r'^2} \iint x\psi \mathrm{d}x\mathrm{d}y$$
$$+\frac{\sin 2\theta'}{4\pi r'^2}\left[\beta \iint y\psi \mathrm{d}x\mathrm{d}y + \iint (\psi_y^2 - \psi_x^2)\mathrm{d}x\mathrm{d}y\right] + \ldots$$

From this we can see that if the disturbance is isolated at all times so that $\psi_t = o(1/r^2)$, not only will $\iint \psi \mathrm{d}x\mathrm{d}y = 0$, but also

$$\iint x\psi \mathrm{d}x\mathrm{d}y = 0$$

$$\iint (\beta y\psi + \psi_y^2 - \psi_x^2)\mathrm{d}x\mathrm{d}y = 0$$

(This can also be shown directly for isolated features by taking x^2, xy and y^2 moments of the vorticity equation.) If the initial state has $\iint \psi \mathrm{d}x\mathrm{d}y \neq 0$, the tendency field is clearly $o(1/r)$ so that the eddy cannot remain isolated, and the boundary integrals cannot be zero. The evolution of the eddy in this case will be influenced by far field effects: it may radiate energy or split into several vortices or evolve in some more complex fashion. This derivation proves that the initial condition, $\iint \psi \mathrm{d}x\mathrm{d}y = 0$, is necessary for isolation, but not sufficient.

The reason why there is an important contribution to the boundary terms when $\iint \mathrm{d}x\mathrm{d}y\psi \neq 0$, even if ψ is initially isolated, is due to the infinite propagation speed

$$c = -\frac{\beta}{k^2 + l^2}$$

for Rossby waves when the wavenumbers k and l go to zero. The Fourier amplitude for this mode ($k, l \to 0$) is proportional to $\iint \psi \mathrm{d}x\mathrm{d}y$.

On the other hand, in a fluid with a free upper surface, the propagation velocities are all finite and therefore we would expect the results above to be modified. We can illustrate the changes in our basic theorem due to free-surface effects by considering the shallow water equations

$$\frac{\partial}{\partial t}vh + \frac{\partial}{\partial x}uvh + \frac{\partial}{\partial y}vvh + fuh = -\frac{\partial}{\partial y}\frac{1}{2}gh^2$$

$$\frac{\partial h}{\partial t} + \frac{\partial}{\partial x}uh + \frac{\partial}{\partial y}vh = 0$$

For a fluid with a free surface, the continuity equation no longer requires that the net linear momenta be zero. In this case, however, we are assured that an initially isolated disturbance will remain isolated for all finite times. Integrating these equations leads to

$$\frac{\partial}{\partial t}\iint \mathrm{d}x\,\mathrm{d}y\,yhv + \iint \mathrm{d}x\,\mathrm{d}y\,yfuh = 0$$

$$\frac{\partial}{\partial t}\iint \mathrm{d}x\,\mathrm{d}y\,yh = 0$$

In order to indicate the modifying effect of a free surface, it suffices to consider only steadily translating disturbances for which

$$\frac{\partial}{\partial t} = -c\frac{\partial}{\partial x}$$

and

$$\frac{\partial}{\partial x}(uh - ch) + \frac{\partial}{\partial y}vh = 0$$

This defines a transport streamfunction in the moving reference frame:

$$vh = [\psi + ch_\infty y]_x,\ uh = -[\psi + ch_\infty y]_y + ch$$

The time derivative term in the momentum equation will vanish, and volume integration gives

$$\beta\iint \psi\,\mathrm{d}x\,\mathrm{d}y = -c\iint f(h - h_\infty)\mathrm{d}x\,\mathrm{d}y$$

so that the mean of ψ clearly is not necessarily zero *. But we can show that the term on the right is small by using a geostrophic scaling $|\psi| \simeq gh_0/f_0|h_0 - h_\infty|$. We then get

$$\frac{\iint \psi\,\mathrm{d}x\,\mathrm{d}y}{gh_0/f_0|h_0 - h_\infty|} \simeq \frac{c}{\beta gh_0/f_0^2}$$

where h_0 is an average depth scale. Since the propagation speed $\beta gh_0/f_0^2$ is 100 m s^{-1} for the ocean, whereas c is closer to 0.05 m s^{-1}, it is clear that the

* This formula explains why Nof (1981) and Ingersoll and Cuong (1981) can obtain purely cyclonic eddies: they are considering only an upper layer overlying a very deep lower layer. Since the speeds obtained are much smaller than the external Rossby wave speed, our theorem shows that either the deeper fluid will have a compensating anticyclonic spin (with weak flows because the layer is thick) or the eddy will not remain isolated. Flierl's (1983) investigation of the full two-layer version of Nof's model showed that under most conditions, the eddy radiated energy as barotropic waves and was not isolated.

net angular momentum must still be nearly zero, so that the theorem is still an extremely good approximation.

The relevance of these ideas to the oceanic eddy complex lies in the fact that dynamical consistency (the angular momentum theorem), as well as kinematical (mass continuity), requires us to recognize the motions in the surrounding water through which an eddy moves. If we want to analyze or model oceanic eddies as isolated entities, then the simplest dynamically consistent unit is the dipole. Naturally, we have no a priori assurance that such a conception will be sound, but one hopes that only near-neighbor (and not the whole ocean!) interactions will suffice for a start.

4. EXPERIMENTAL STUDIES OF EDDY PAIRS

The question naturally arises as to whether the realization of a modon requires a very special kind of excitation, or whether such structures would evolve naturally under rather general forcing conditions. A partial answer to this question is already provided by the experiments of Griffiths and Linden (1981) who observed a vortex pair evolving from the baroclinic instability wave on a density front. This section describes our attempts to realize a modon in the simpler context of a barotropic fluid.

The experiment (Fig. 1) consists of forcing a jet of water to flow horizontally into a 2 m diameter rotating tank of water, and observing the motion downstream from the nozzle. The qualitative pattern to be described

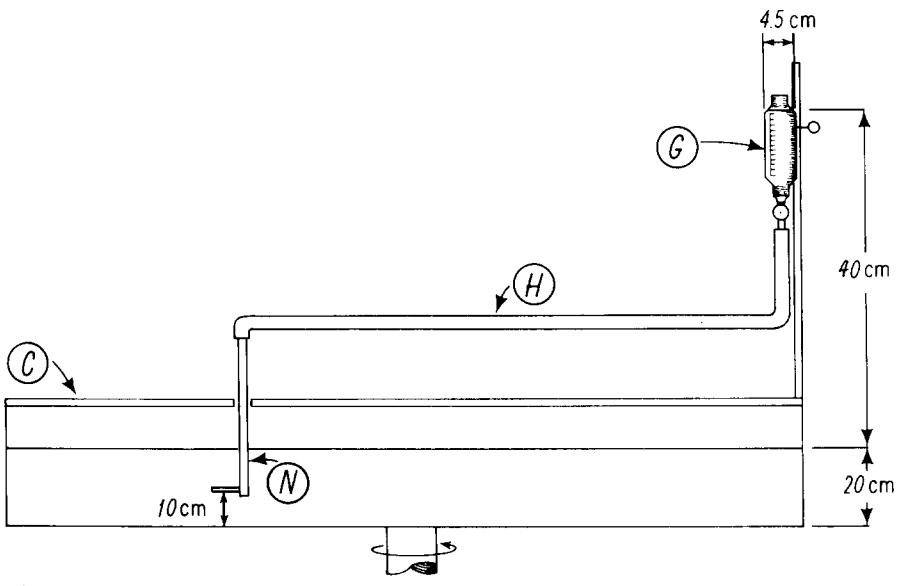

Fig. 1. Sketch of the experimental apparatus.

is independent of the azimuthal and radial position of the nozzle, provided it is far from the rim of the tank, and the pattern is also independent of the vertical height of the nozzle above the bottom. Indeed, in one run we used four parallel nozzles equally spaced throughout the depth of the fluid and obtained qualitatively similar dye patterns. In the quantitative runs (Figs. 3 and 7), the nozzle (0.13 cm i.d.) was 3 cm long in the horizontal direction, and was fed via a graduated cylinder in which the head of water was 40 cm above mean sea level. A pinch valve on the feeding hose allowed us to squirt a small amount of fluid into the tank.

This water had a one percent (by volume) food coloring dye, and the inflow rate was sufficiently large so that a conically symmetric turbulent jet was formed when the tank was not rotating.

The experiment was started by filling the tank to the desired depth, taking care to keep the water temperature below wet bulb room temperature to avoid surface cooled convection currents. After insuring that the water was fully spun up at a counterclockwise period of 15 s, an eddy was generated by releasing the pinch valve and allowing the dyed water to emerge from the nozzle for 15 s.

The incoming conical jet is deflected by the Coriolis force and starts to accumulate in an anticyclonic vortex (Fig. 2a, b) *. A Taylor–Proudman adjustment at this stage is also visible in the columnar structure of the spreading dye in the vortices, i.e., the three-dimensional turbulent motions in the jet give way to two-dimensional and more-ordered motions. The jet feed has been turned off before Fig. 2c, and we see the beginnings of a large cyclonic vortex on one side of the original anticyclone, together with the emergence of a smaller cyclone. The subsequent figures show a fully formed modon pair moving away from the source region and detaching from the small cyclone. The modon invariably moves in a curved path, and sometimes collides with the small cyclone (Fig. 2h, i). In some runs the small cyclone would pair up with the anti-cyclonic vortex in the modon.

Although we do not know why the "mother" vortex (the anti-cyclone) gives birth to the "father" vortex (the larger cyclone) or to the "son" of modon (the smaller cyclone), we may note that the incoming jet has equal amounts of cyclonic and anti-cyclonic shear, so that there is a source region for the cyclones which form outside the circumference of the anti-cyclonic eddy. The turbulent entrainment on the outside of the clockwise turning jet might provide the mechanism for the relatively low pressures in the father and the son. Furthermore, we note that in the absence of rotation, the

* For the qualitative runs, (Figs. 2 and 8), the nozzle was only 4 cm above the bottom. Other conditions were similar.

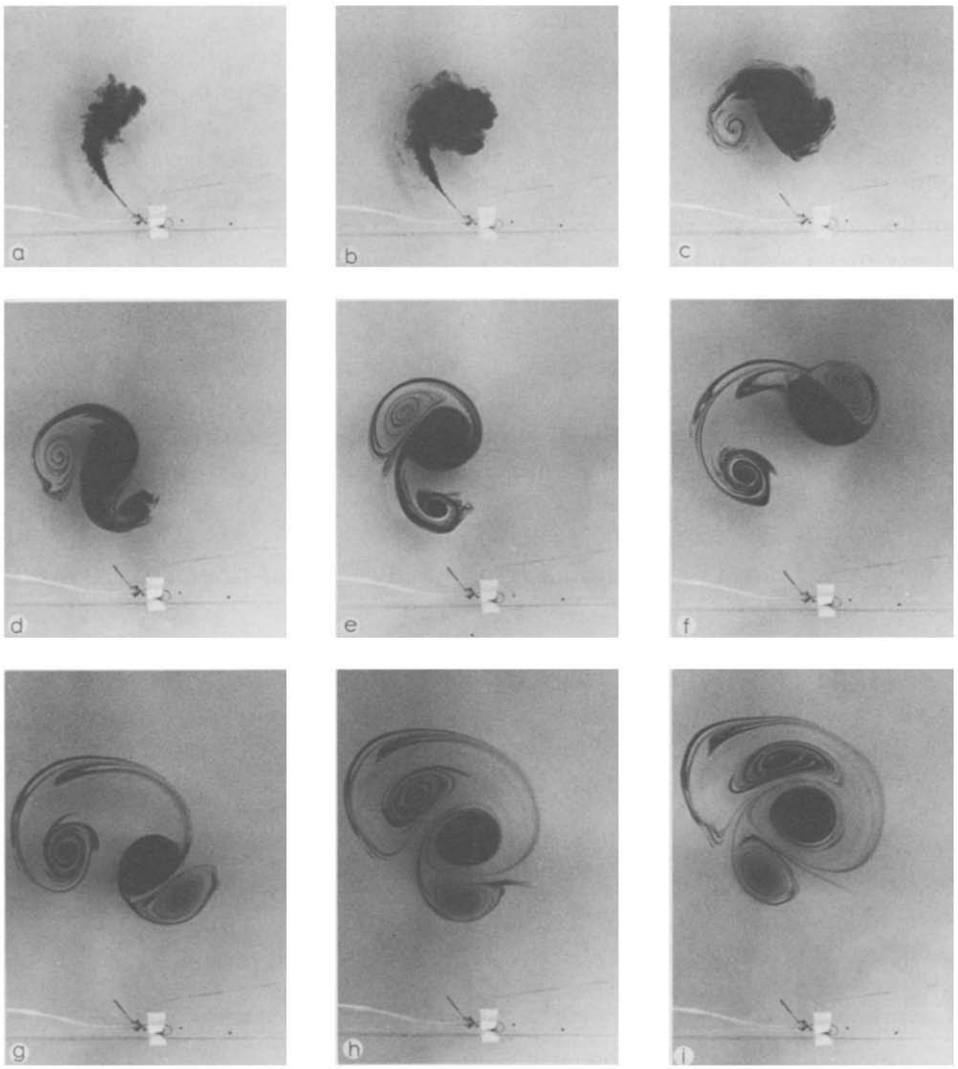

Fig. 2. The evolution of a typical eddy pair generated by a turbulent jet. When the inflow is started, a three-dimensional jet (a and b) emerges and curves to the right in approximately an inertial circle. The inflow is stopped (c) and a large cyclonic vortex is formed on the left side of the anticyclone. The fully formed two-dimensional eddy pair (e) then propagates away from the source (f and g), and finally collides with the eddy left behind, severely distorting it in the process (h and i). The times for the above frames are 7.5, 15.1, 30.2, 45.3, 60.4, 105.7, 151.0, 170, and 196.3 s after start, respectively. The period of rotation was 15.1 s.

entrainment by the jet would create two relatively weak secondary circulations on either side of the jet and extending over the entire basin. Apparently, the rotation modifies these secondary circulations so that their

lateral dimensions are not controlled by the walls of the tank, but appear instead as a modon and a vorticity-compensating son.

The resulting modon is remarkably regular considering either the turbulent jet or the nebulous anti-cyclone which first forms. The time of modon formation is only about two tank revolutions, which suggests that the β-effect is not important. This inference is supported by the observation that the qualitative structure is the same even if we place the nozzle at the center of the rotating basin. Therefore, Batchelor's (1967) solution for a vortex pair might provide a model of the fully developed modon, except for the fact that the latter moves in a curved path and leaves the son behind.

Measurements of the velocity structure of the modons were obtained as follows. The tank was covered with a Plexiglas lid before spin-up to minimize surface stress due to air drag. After the water was fully spun up, the run was started by carefully removing the lid over the quadrant of the tank with the nozzle, strewing some paper pellets on the exposed free surface, and releasing the pinch valve for the 15-s interval. The flow was recorded by taking movies of the floats against a black tank bottom. The form of the eddies was also further revealed by dye as in Fig. 2, but this time the dye was a fluorescent one.

Figure 3 shows six different float paths. The outline of the dyed region at the initial instant is shown as a lightly drawn curve. The anticyclonic eddy was well developed as could be seen from the dye. Also, the cyclonic eddy

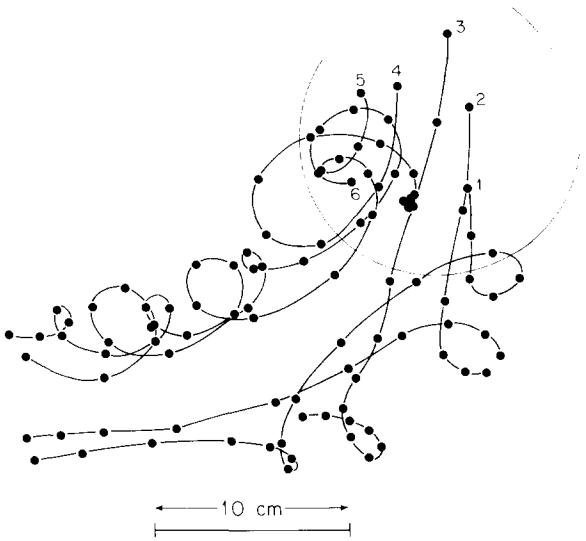

Fig. 3. Paths for six floats in the modon. Dots were made every 3.1 s. Starting time was 60 s after the start of the experiment. The outline of the dyed region at the initial instant is shown as a light curve.

was almost completely formed. Float 5 was in the anticyclonic eddy and showed the largest epicyclic motion. Float 6 is nearer to the center and exhibited a smaller epicyclic path. Both stayed in the anticyclonic eddy for the duration of the observation—more than three revolutions. Float 4 was left behind in the tail after one rotation. Floats 1, 2 and 3, on the other hand, show the motion in the cyclonic eddy. Float 2 ended up near the axis of the modon. Floats 1 and 2 exhibited weaker epicyclic flow than the floats in the anticyclonic eddy.

The difference between the circulation of the two eddies is particularly illustrated by the two trajectories, W4 and S5 in Fig. 4. (The nomenclature is purely for reference to the original films.) We selected these tracks as being representative of the maximum epicyclic motion. Float S5 is in the cyclonic and W4 is in the anticyclonic eddy. The initial time for all trajectories in this

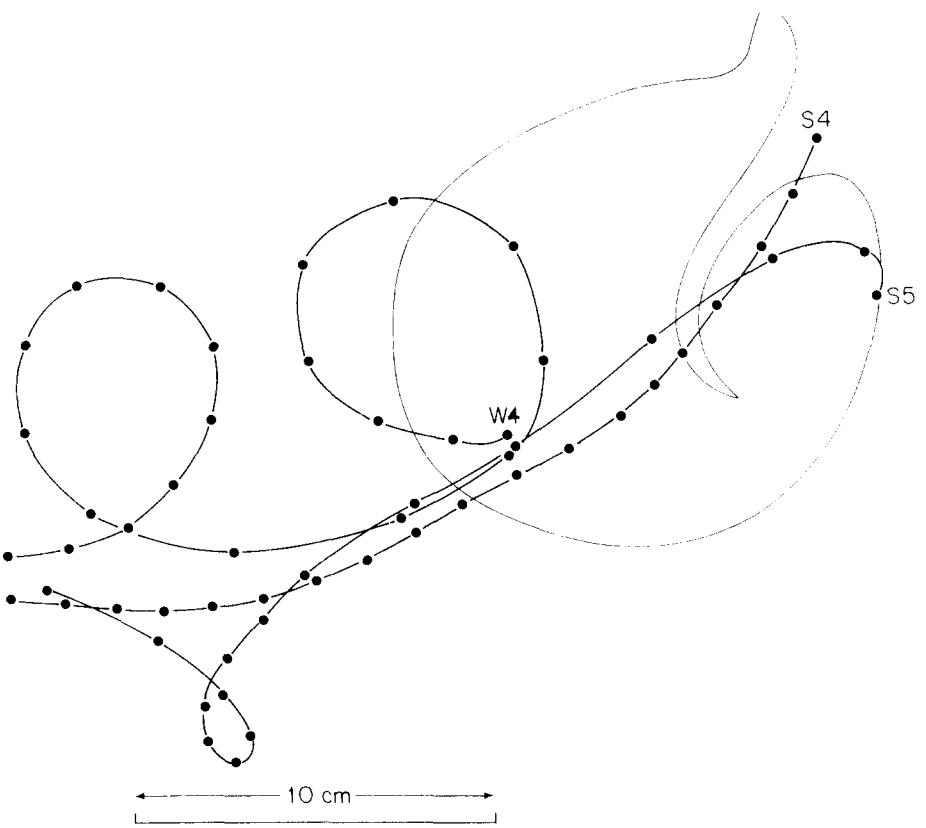

Fig. 4. Two trajectories which exhibit the typical epicyclic motion of the two vortices. The light curve outlines the position of the dye at the initial instant (52 s after start). Time between dots was 35.1 s.

figure is 52 s after the start. Also shown is Float S4 which has no epicyclic motion. It was consistently located outside, but near the trailing edge of the modon and is a good indication of the mean motion of the modon.

Figure 5 shows three particles which were originally outside the eddies. One particle (No. 9), was initially at the nose of the leading edge of the modon (almost exactly at the interface between the dyed/non-dyed region). This particle was entrained by the anticyclonic eddy. Another particle (No. 7) which started out in a region before the eddy pair, was not entrained, but instead was pushed aside and exhibited a little loop as the modon passed. Also shown in Fig. 5 is the outline of the dye at the last frame. Note the tail, where particle No. 7 ended up. Figure 5 also shows a particle (No. 8) which is initially ahead of the anticyclonic eddy and which also ended up left behind in the tail. The S-1 and W-1 floats in Fig. 6a, b, together with the dye outlines, illustrate the correspondence of the epicyclic motion to the dye patterns. The starred points 1, 2 and 3, give the float positions in relation to the dye outlines at these times. The entire data set is consistent with an isolated and coherent pair of eddies propagating through the surrounding fluid.

Figure 7 shows an instantaneous picture of the velocity vectors for the entire field. This was obtained by recording the position of pellets at one instant in the movie (at approximately 60 s after the jet was first turned on).

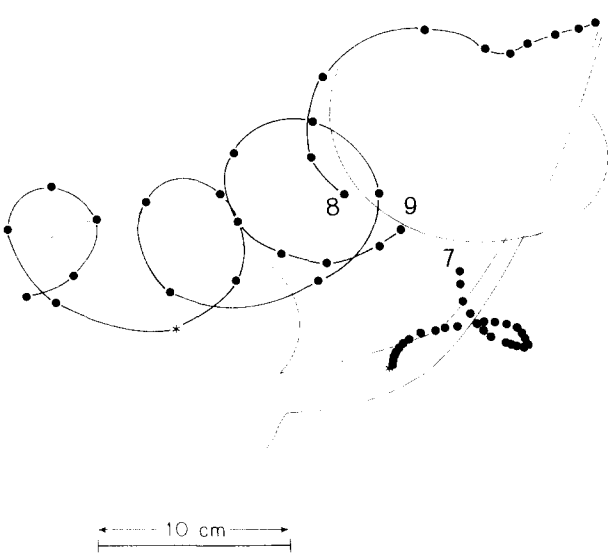

Fig. 5. The trajectories of three particles which were near, but possibly in front of the eddies. Particle 9 was entrained into the anticyclonic eddy. Particles 7 and 8 were deflected around the eddy and ended up in the region near the tail. Time between dots was 3.86 s.

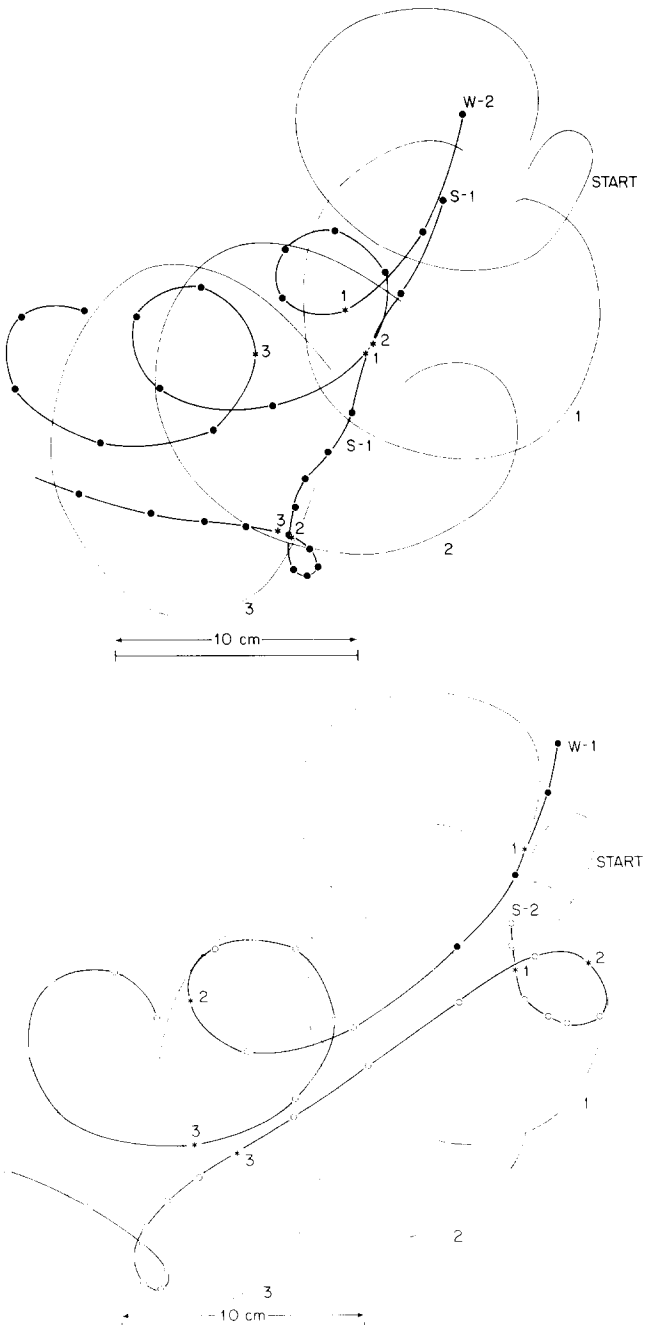

Fig. 6. Particle trajectories and their relation to the dyed region of the modon. The light outlines labeled start, (60 s into the run), 1, 2, and 3 correspond to the outline of the dye at particular times. The position of the particles at times 1, 2 and 3 are indicated by numbered stars.

Fig. 7. Velocity vectors obtained by recording the traverse of the pellets over a 10-frame interval. This is a typically mature modon, approximately 60 s after the start of the experiment.

and then advancing the movie ten frames, recording the position with another colored pen, and connecting the centers of the two pellet images. Great care was taken to eliminate frame jiggle by carefully overlaying selected pellets far from the modon, which had been observed to be motionless in the movie. The error in measurement is estimated to be less than two thicknesses of the cross line. A larger error arising from the decoupling of the surface flow and the interior flow by surface tension is possible, this effect being most extreme in float stagnation regions of high divergence or convergence. However, inspection of the movies and comparison of the movement of pellets with motion of the dye when the flow has become two-dimensional, indicate the pellets follow the interior flow closely. The data in Fig. 7 will be compared with theoretical models later.

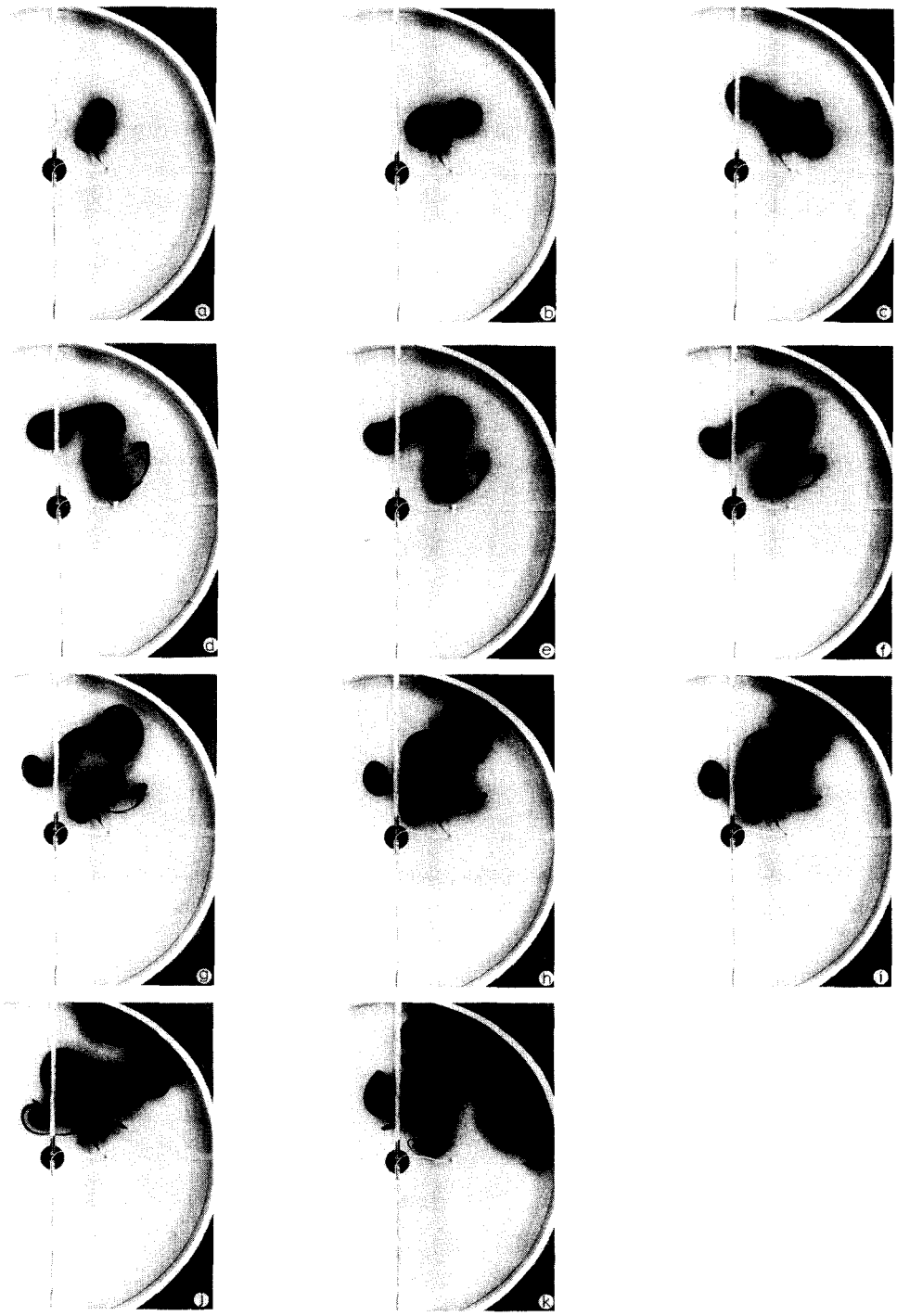

Fig. 8. The evolution of the eddy field with time under conditions similar to Fig. 2. At about 75 s, the first eddy pair begins noticeably to leave the generation region (a). By 105 s, the first

There is a striking difference between this kind of free jet flow and the flow from a source located near a vertical wall (coast). In the latter case, the flow can easily proceed away from the source in a geostrophic coastal current because of the pressure support afforded by the boundary. No such support exists for our free jet, and the line integral of the pressure gradient along circles surrounding the nozzle vanishes. The preceding experiment suggests that dipole interactions are very important for transporting the incoming water away from a "free" source; otherwise the incoming jet would accumulate in a large anti-cyclone near the nozzle, and only Ekman friction would be available to spread the water over the rest of the tank.

The question then arises as to the nature of the outflow from the nozzle when the inflow is maintained continuously (Fig. 8). Upon starting this run, a first modon pair (Fig. 8a) forms in the same fashion as in the pulsed cases (Fig. 2). Some time later, a second modon pair is observed to form and move off to the left (Fig. 8b, c). This appears to originate with the "son" giving birth to his own wife. Subsequent eddies form from the jet but do not generally pair as systematically (Fig. 8d–k), and we have a truly two-dimensional turbulent region in which much of the transport occurs through stochastic vortex pairing rather than by Ekman friction. An important integral constraint pertaining to this turbulent flow will be derived in Section 7.

5. A VORTEX PAIR MOVING IN A CIRCULAR PATH

The qualitative and quantitative experiments give convincing evidence that a coherent dipole is formed in the initial stages, and we shall now show that the path curvature is consistent with the observed asymmetry between the high and low pressure centers. The experiments suggest, as previously mentioned, that neither the free surface deformations nor the β-effect induced by the mean parabolic shape of the surface are particularly important. Furthermore, the parameter which measures the quantitative importance of the β-effect in the vorticity equation is

$$\frac{\beta L^2}{U} = \frac{1}{4}\frac{fR}{R_d^2}\frac{L^2}{U}$$

---

modon has moved off to the right (b) and travels in a circular path (c). The second modon moves to the left (d). Other interesting events are the intersection of the first modon and jet (d, e and f), the collision of two modons (g and h) and the effect of the wall (i and j). Although the excessive dye (and the wall) obscures the pattern (k), the picture we get is that the scale of the two-dimensional eddies increases with distance from the source within a "wake" angle considerably larger than without rotation. Times after start for a–k are, respectively, 75, 105, 150, 195, 210, 225, 240, 270, 285, 360 and 540 s.

where R is the tank radius of 1 m, R_d is the radius of deformation (1.6 m), and U is the typical particle velocity in the modon. Using values of the latter obtained from Fig. 7, we find that $\beta L^2/U \sim 0.01$ and conclude that the β-effect is negligible.

Therefore, we need only consider the two-dimensional vorticity equation

$$\frac{\partial}{\partial t}\nabla^2\psi + J(\psi, \nabla^2\psi) = 0$$

The simplest case which is relevent to the laboratory experiment consists of three-point vortices: an anticyclone paired with a slightly weaker cyclone and a third cyclone representing the son. Since no net relative vorticity is transported with the jet, the sum of the strengths of the three vortices will be chosen to be zero

$$\sum_{i=1}^{3} S_i = 0$$

where the streamfunction can be expressed as

$$\psi = -\sum_{i=1}^{3} S_i \ln|\mathbf{x} - \mathbf{x}_i|$$

The evolution of the positions $\mathbf{x}_i$ of the vortices, calculated in the standard way, is shown in Fig. 9 for the case when the three-point vortices are originally arranged in a triangle. Note how the pair moves away from the weaker "son" vortex and translates in a circle with little influence from the son, which becomes almost stationary. The subsequent evolution is also interesting: the pair returns from behind to interact with the son which makes one loop about the mother and diverts the pair into a different direction, with the whole sequence beginning again (Fig. 9c). Perhaps this is analogous to the more complex interaction seen in the laboratory (Fig. 2h).

The next simplest case corresponds to a modon with a continuous distribution of vorticity but with non-zero circulation around the exterior, and we will obtain a dipole solution with unequal strength low and high centers. The point vortex model suggests that this solution, which has, as yet, no feature corresponding to the son, should be satisfactory during the phase of the motion where the pair is widely separated from the son and is moving steadily in a circle. The suggestion is confirmed by a subsequent argument.

Let us, therefore, start by constructing an exact solution to the vorticity equation which is stationary in a coordinate system rotating clockwise with angular frequency Ω. Using polar coordinates (R, θ) relative to the center of rotation in the vicinity of the son, the solution sought is

$$\psi = \psi(R, \theta + \Omega t)$$

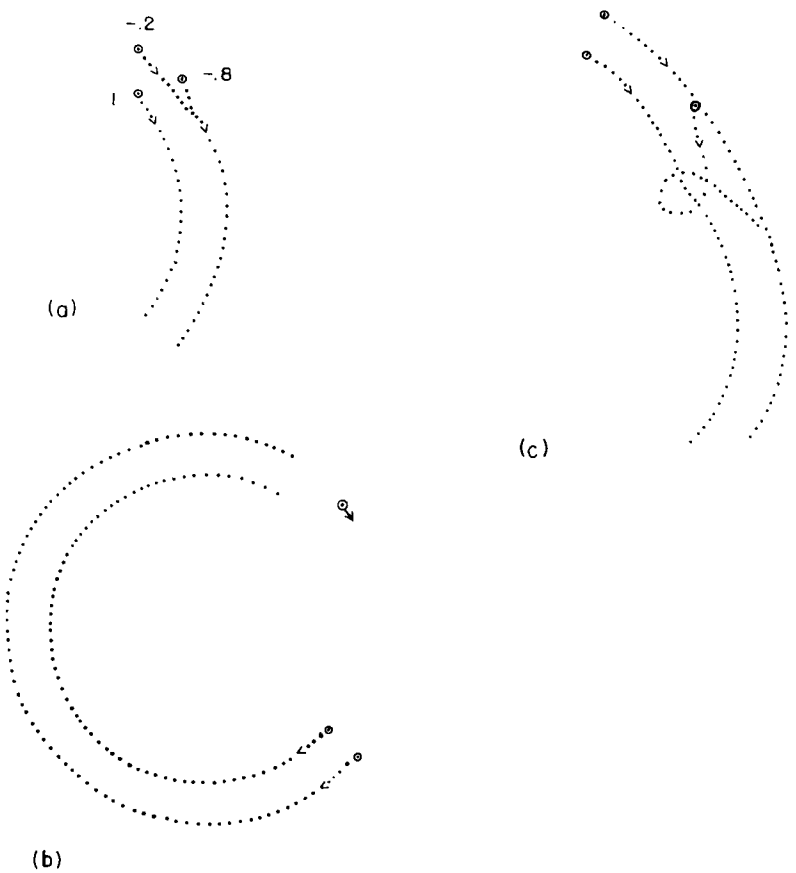

Fig. 9. Tracks of three point vortices. (a) The circled positions are the initial locations of the vortices with the labels being the strengths s_i. (b) Continued tracks showing the circular track of the pair with the "son" being almost stationary. In this regime, the continuous models shown in Fig. 11 should be accurate representations of the flow field and the motion of the pair. (c) Subsequent interactions of the pair with the "son".

and the vorticity equation becomes

$$J\left(\psi + \frac{\Omega R^2}{2}, \nabla^2\psi\right) = 0$$

If a is the modon radius, $R = a/\epsilon$ the modon center (Fig. 10) and (r, ϕ) denote polar coordinates relative to this center, then

$$J\left(\psi + \Omega\frac{a}{\epsilon} r \sin\phi + \frac{\Omega r^2}{2}, \nabla^2\psi\right) = 0$$

Rewriting Ω in terms of the speed of motion along the track c, $\Omega = c\epsilon/a$ gives

$$J\left(\psi + cr\sin\phi + \epsilon\frac{cr^2}{2a},\ \nabla^2\psi\right) = 0$$

For any function, $F(z)$, a solution of this equation is

$$\nabla^2\psi = F\left(\psi + cr\sin\phi + \epsilon\frac{cr^2}{2a}\right)$$

In the exterior of the modon ($r > a$), the vorticity is zero so that

$$\psi = B\frac{a}{r}\sin\phi + M\ln\frac{r}{a}$$

The quantity $\psi + cr\sin\phi + \epsilon cr^2/2a$ gives the streamfunction for the velocity relative to an observer rotating with the modon, and since this streamfunction must be constant on $r = a$, we have

$B\sin\phi + ca\sin\phi + \epsilon ca/2 = \text{constant}$

and therefore

$B = -ca$

$\text{constant} = \epsilon ca/2$

In the interior of the modon, we can choose F arbitrarily and will follow the usual simple procedure of selecting a linear function, viz.

$$F(z) = -k^2(z - \epsilon ca/2)$$

The constant term here matches the interior vorticity to the exterior value

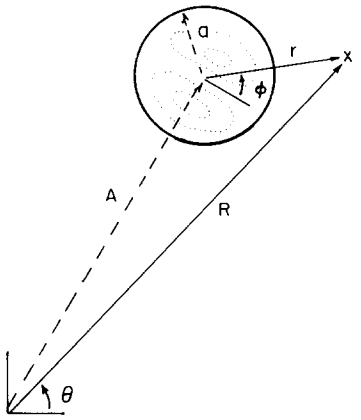

Fig. 10. Geometry of solutions for a modon moving in a curved path, showing radius of track ($A = a/\varepsilon$), radius of modon (a) and the tank-centered (R, θ), or modon-centered (r, ϕ), co-ordinate systems.

($F = 0$) at the bounding streamline $z = \epsilon ca/2$. The solution to the interior equation

$$(\nabla^2 + k^2)\psi = -k^2 cr \sin\phi + \epsilon \frac{ck^2}{za}(a^2 - r^2)$$

is

$$\psi = -cr \sin\phi + DJ_1(kr) \sin\phi + \frac{\epsilon c}{2a}(a^2 - r^2) + \frac{2\epsilon c}{k^2 a} + EJ_0(kr)$$

The first matching condition, that $r = a$ be a streamline in the rotating system

$$\left[-ca + DJ_1(ka) + ca\right] \sin\phi + \frac{2\epsilon c}{k^2 a} + EJ_0(ka) + \frac{\epsilon ca}{2} = \frac{\epsilon ca}{2}$$

leads to the dispersion relationship

$$J_1(ka) = 0 \Rightarrow ka = 3.83$$

and to

$$E = -\frac{2\epsilon c}{k^2 a J_0(ka)}$$

a positive constant.

Finally, we match the tangential velocity to satisfy continuity of pressure, leading to

$$D = \frac{2ca}{kaJ_0(ka)}$$

$$M = -\epsilon ca$$

so that the final solution is

$$\psi = ca \begin{cases} -\dfrac{a}{r}\sin\phi - \epsilon \ln\dfrac{r}{a} & r > a \\ \left[\dfrac{zJ_1(kr)}{kaJ_0(ka)} - \dfrac{r}{a}\right]\sin\phi + \dfrac{2\epsilon}{k^2 a^2}\left[1 - \dfrac{J_0(kr)}{J_0(ka)}\right] + \dfrac{\epsilon}{2}\left[1 - \dfrac{r^2}{a^2}\right] & r < a \end{cases}$$

where $ka = 3.83$ and ϵ is the ratio of the modon radius to the radius of its track. In Fig. 11, we show contours of the streamfunction ψ in the tank frame and in the modon frame $[\psi + cr \sin\phi + \epsilon r^2/2a^2]$ for various ϵ values ($c = 1$). These show clearly the asymmetry of the mother and father and the curvature of the modon path which obviously depend upon the finite value of the circulation about an exterior contour, i.e., in the region where the vorticity is zero.

It only remains for us to remark on the connection (as indicated previ-

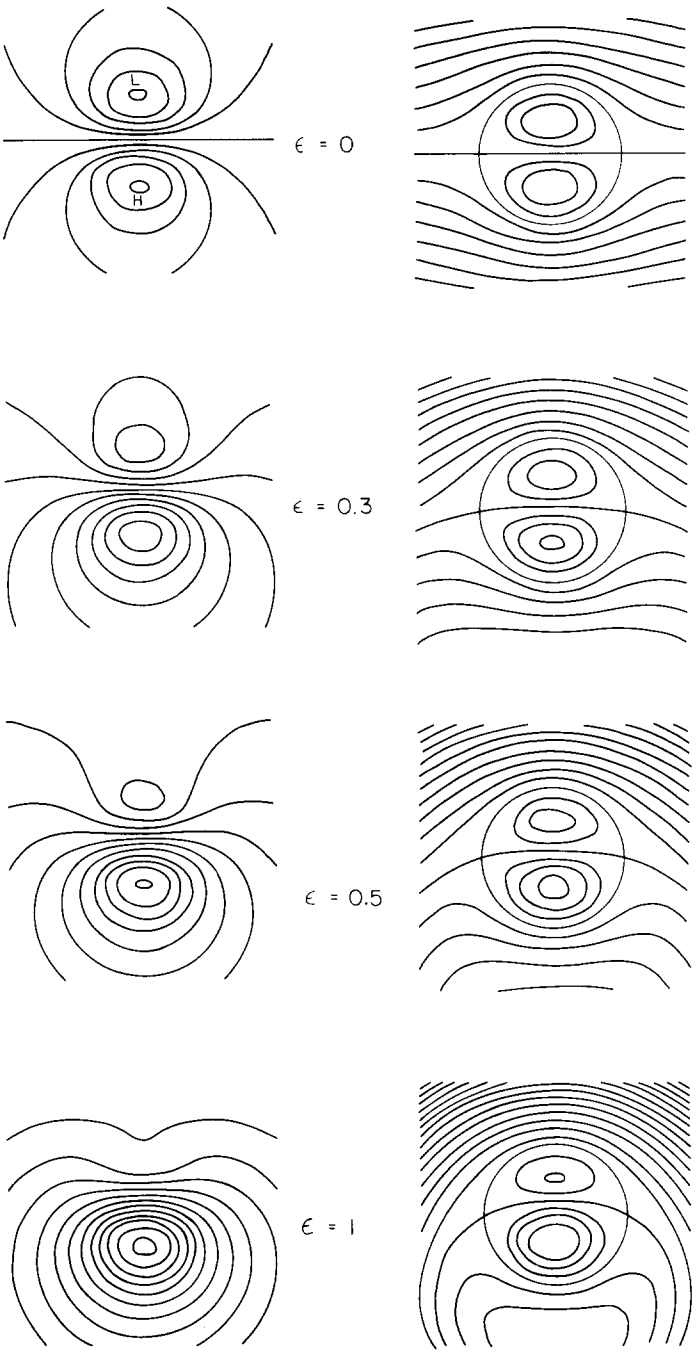

Fig. 11. Streamfunction of the flow for various ϵ values. The left-hand contours are in the tank frame of reference while the contours on the right show streamlines relative to the eddy. Note the intensification of the high and weakening of the low as the path curvature becomes greater. Contour intervals are 0.25.

ously) of this solution with the continuous three vortex problem. An asymptotic expansion ($\epsilon \ll 1$) has been found (but not included herein) when the separation between the modon and the son is large (order $1/\epsilon$) compared to the radius of the modon. Under these circumstances, the currents induced by the son, which itself is basically a simple cyclone of strength ϵ, will be very weak [$0(\epsilon^2)$] near the modon. The solution given above is then valid to order ϵ^2 near the modon; including the next order gives the small effect of the son on the propagation of the modon and vice versa. To examine further the structure of the flow or to consider the case when $\epsilon \sim 1$, numerical work seems necessary (perhaps using the methods of Deem and Zabusky, 1978).

6. COMPARISONS WITH THE EXPERIMENTS

The laboratory experiments we have described clearly involve many different and complex phenomena: the 3-D turbulent jet turning in an inertial circle; the formation of 2-D Taylor columns; the geostrophic adjustment; the evolution of a vortex pair from the amorphous cloud; the motion of the pair; and (in the continuous inflow cases) the formation of successive vortices with their irregular pairing and separating. The simple model discussed above is relevant to only a very small part of the whole problem, viz., the description of the motion of the vortex pair. We cannot, therefore, expect detailed quantitative agreement between the model flow field and the observed fields, but we will show that certain essential features of the laboratory modons are described by the simple model.

In this section, we shall show that the laboratory modons:

(1) are strong vortices which carry fluid with them in their motion;

(2) translate due to the internal dynamics of the eddies; and

(3) move in curved paths because of non-zero net vorticity within the pair.

The first property, transport of a volume of water, is clearly shown in the dye photographs. A large fraction of the injected dyed fluid is carried away from the nozzle by the modon. In addition, entrained clear fluid also appears to be transported with the eddy in the father vortex. The dipole volume is approximately 2400 cm^3—about 100 times the volume actually injected into the tank. The float tracks (Figs. 3–6) also show the cycloidal tracks characterizing a particle caught within a circulating and translating body of fluid.

The second point, that the translation is a dynamical result of the vortex pair interaction, is more difficult to demonstrate. Particle number 7 in Fig. 5 shows clearly the translation of the pair relative to the surrounding fluid. For a more quantitative comparison, we first show that the period for the floats is consistent with those predicted by the modon model. The periods of the floats shown in Figs. 3–6 range from 16.4 to 41.5 s. In the model solution,

this period depends on the distance of the float trajectory from the high or low center (as viewed in the frame of reference moving with the eddy). We have calculated the circulation time for the simple Batchelor vortex by integrating the Lagrangian equations; the results are that

$$T \geq 1.3\frac{a}{c}$$

which corresponds to a lower bound on T of 18 ± 3 s using $a = 6.1 \pm 0.5$ cm and $c = 0.45 \pm 0.5$ cm s^{-1}. This period pertains to floats located near the high or low center. For particles farther out, the period may be a factor of two larger if the maximum excursion of the float is about 90% of the radius; thus the observed periods are quite consistent with the theoretical periods.

Another calculation which indicates that the currents in the pair are strong enough to account for the vortex movement is a comparison of the flow speed in the center of the eddy with the translation rate. From the flow vectors in Fig. 7, we estimate the maximum particle speed is 1.8 cm s^{-1}, while the eddy moves at 0.45 cm s^{-1}. The ratio of these two is in reasonable agreement with the value

$$U_{max}/c = \frac{1}{J_0(k)} + 1 = 3.5$$

predicted for the Batchelor modon ($\epsilon = 0$ case).

These calculations suggest that the currents are indeed strong enough to account for the translation of the dipole. The fact that it moves in a circle appears to be associated with negative net vorticity within the modon. Our theory suggests that the net circulation on a contour enclosing the modon will be

$$\oint \mathbf{u} \cdot \mathbf{dl} = -2\pi ca\epsilon$$

as computed from the logarithmic term in ψ. For this experiment, we obtain

$$-2\pi ca\epsilon = -8.4 \pm 4 \text{ cm}^2 \text{ s}^{-1}$$

using $a = 6.1 \pm 0.5$ cm and $A = 11$–16 cm, giving a value of $\epsilon = a/A$ of 0.3–0.5. The circulation integral in the above equation has been computed using the velocity vectors in Fig. 7 and a circular contour of radius 7.6 cm. The resulting directly measured net circulation is

$$\oint \mathbf{u} \cdot \mathbf{dl} = -10.6 \text{ cm}^2 \text{ s}^{-1}$$

The agreement of the last two equations is again encouraging: it is clear that the vortex pair has net negative vorticity of the right size to account for the circular paths. These order of magnitude comparisons suggest that even our

highly idealized model does capture many features of the evolution of the flow. Modons appear to be easily realizable and natural elements of inertial flow in a rotating system.

7. SUMMARY AND SUGGESTIONS

We have shown that a modon consisting of opposing vortices with unequal strength is able to account for the evolution of the motion when a small amount of fluid is squirted into the rotating tank. We are confident that similar results would be obtained using a vertical line source (rather than a point or nozzle), in which case the motion would be two-dimensional from the start.

It is interesting to recall that the two-dimensional vorticity equation "governs" the motion on the f-plane, and the Coriolis parameter does not appear in this equation. The boundary conditions at the nozzle or at a vertical line source are also the same as in a non-rotating system, and we have an interesting paradox because the solutions of the vorticity equation do not "know" that the fluid is rotating! Something is clearly missing from the vorticity equations (and the aforementioned inlet conditions) because the following simple argument (based on the momentum equation) is indeed sufficient to explain the observed circular path of the incoming jet and its obvious dependence on f. We balance the Coriolis force with centrifugal force, assuming a laminar flow $\mathbf{u} = v(r)\hat{\theta}$ with no net pressure difference across the radial (r) extremities of the jet. Thus, the integrated momentum equation across any section of the jet yields

$$\int \mathrm{d}r \frac{v^2}{r} + f \int \mathrm{d}r\, v = 0$$

from which we obtain the important scale length

$$R_f \sim -\frac{f \int \mathrm{d}r\, v}{\int \mathrm{d}r\, v^2}$$

as a function of the input velocity profile and the Coriolis parameter. This determines not only the radius of curvature of the jet, but also the lateral dimension of the first (anti-cyclonic) vortex which forms. It probably also determines the scale of the smallest eddy in the two-dimensional turbulent jet which results (Fig. 8) when there is a continuous inflow, as discussed further at the end of this section.

Although we have no firm explanations of the process by which the "father" vortex forms from the "mother", one speculation has already been

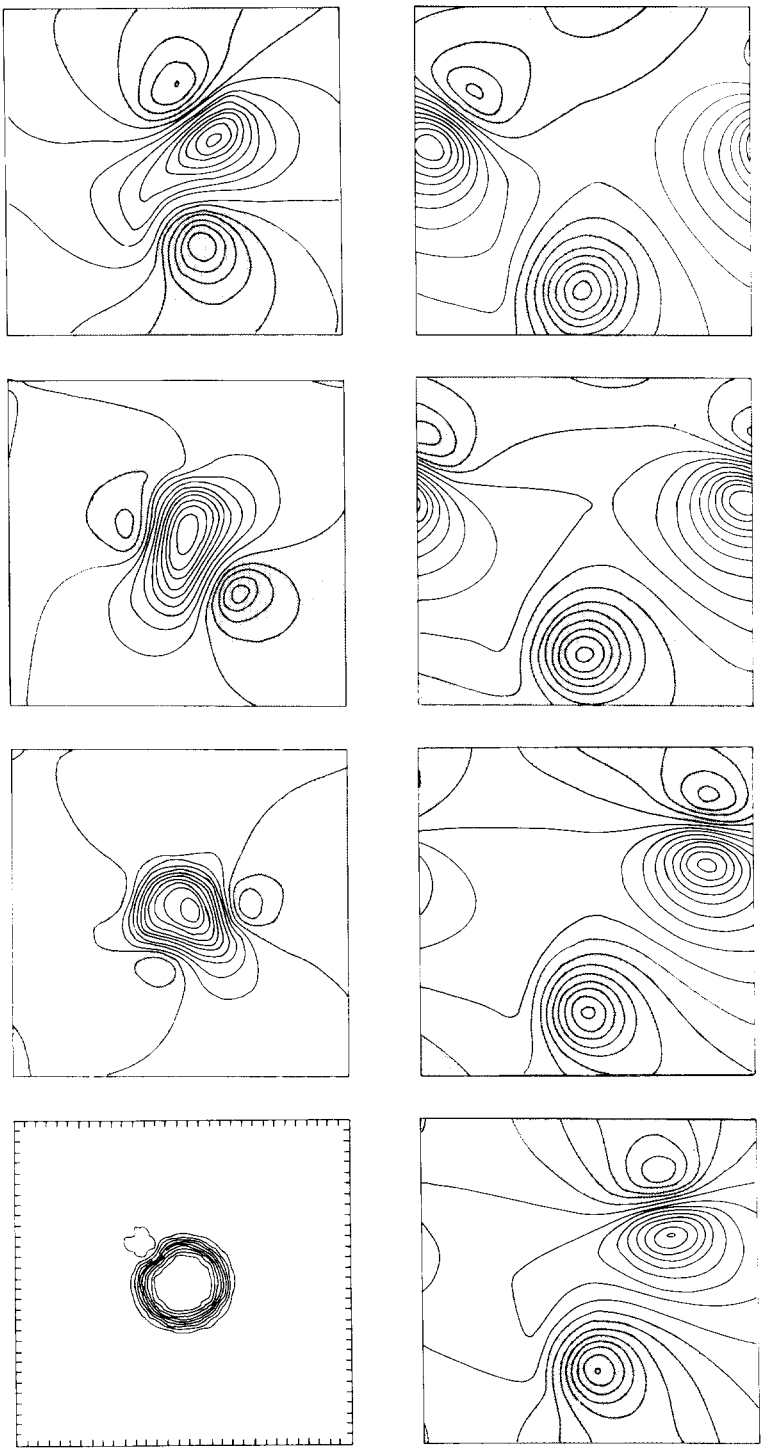

Fig. 12. Instability of an initial state shown in the first frame. Streamfunction contours are presented every 200 time-steps. The periodicity of the domain is noticed in the last two frames where the modon is disappearing to the south and reappearing from the north.

offered—that the entrainment process produces a cyclonic circulation.

A second possibility is that the mother vortex is unstable. A preliminary numerical experiment, integrating the 2-D vorticity equation forward in time from the initial state shown in Fig. 12, does show the formation of a dipole pair with a son vortex left behind. The initial condition was chosen to represent a geostrophically adjusted mother vortex with some perturbations left from the inflow. Since we suspected the scale of the modon would be closely related to the width of the initial azimuthal current (and mindful of the Rayleigh stability criterion), we chose to try a fairly stagnant, high-pressure interior with a somewhat narrow band of current around the outside. The total length of integration shown is about seven turn-around times of the initial vortex. The numerical calculations are performed with a 32×32 pseudospectral model in a periodic domain with biharmonic friction. Other initial conditions give similar results: the vortex breaks up into several eddies. Obviously, there are many questions and further experiments suggested by this calculation; we only show this example as evidence of the plausibility that instability may lead to dipolar structures. In addition, we note that Firing and Beardsley (1976) generated experimentally an initial state similar to this and observed that the flow field relaxed to a more dipolar structure.

Finally, we would like to exhibit an important integral constraining the statistically steady turbulent jet in a rotating system (Fig. 8). Using polar coordinates centered on the nozzle, with u as the radial and v as the azimuthal component, we have the constancy of mass flux

$$M = \left\langle \int_0^{2\pi} \mathrm{d}\theta \int \mathrm{d}z \rho_s r u \right\rangle$$

where the z integral is over the entire depth and the brackets denote a time average over the statistically steady state. Integrating the azimuthal momentum equation yields

$$\left\langle \frac{\partial}{\partial r} r \int_0^{2\pi} \mathrm{d}\theta \int \mathrm{d}z (\rho_s u v) \right\rangle + \left\langle \int_0^{2\pi} \mathrm{d}\theta \int \mathrm{d}z (\rho_s u v) \right\rangle = -fM + \left\langle \mathcal{F} \right\rangle$$

where $\mathcal{F}$ is the net friction (Ekman) force in the azimuthal direction. If we neglect $\mathcal{F}$ (for a deep inertial fluid with largely compensating cyclonic and anti-cyclonic viscous forces) as a first approximation, then the solution of the differential equation above is

$$\left\langle \int_0^{2\pi} \mathrm{d}\theta \int \mathrm{d}z \rho_s u v \right\rangle = -\frac{fM}{2}$$

where we have used a boundedness condition at the origin ($r = 0$). This

equation, which merely expresses the constancy of the outward flux of total angular momentum, supplies a prediction of the turbulent Reynolds stress at moderate distances from the nozzle when the outflow is continuous and the tank is large (e.g., Fig. 8). Clearly, the mean flow (M) is not geostrophic, although the velocities which contribute to the eddy stress term may be quasi-geostrophic.

If the u, v correlation is independent of viscosity, then a similarity argument (assuming a turbulent wake angle θ independent of r) yields

$$|u'|\alpha|v'|\alpha\sqrt{\frac{fM}{\rho_s H}}$$

for the r.m.s. horizontal velocity, where H is the depth of the fluid and the coefficients of proportionality are universal. These velocities are large compared with the mean, $u \sim M/\rho_s Hr$, at large r ($r > R_f$), a result which is consistent with Fig. 8. In this turbulent run, we suggest that the outward transport of dyed fluid occurs as the strong eddies intermittently pair and jostle each other outwards. The effect is quite different from that which would be observed with monopolar eddies having no self-propulsive mechanism and being much less effective in tracer transport. The differences between our experiment and non-rotating turbulent jet flow are striking, since there are no constraints on the mean radial outflow in the latter case and the fluctuating velocities are a smaller fraction of the mean flow than in the rotating case.

The vortices in our experiment produce eddies of larger size as the distance from the nozzle increases. Often, intermittent dipole formation can be seen, and the "cascade to larger scales" appears to be connected with dipole structures. Although such structures need not be ubiquitous, we believe that our experiment demonstrates that modons are important in certain, homogeneous f-plane turbulent flows and our theorem indicates that they should play an even stronger role on the beta plane. They can be generated from conditions with no resemblance to a dipole and they can be very efficient in long-range transport of both passive and dynamical properties.

ACKNOWLEDGMENTS

This work was supported by grants from the O.N.R. (M.S. and J.W.) and the N.S.F. (G.F.). Robert Frazel provided essential support for the experimental work, William Dewar supplied the program for the numerical integrations and Anne-Marie Michael typed the text. In addition to these, we would also like to thank the G.F.D. programs (1981, 1982) at Woods Hole for providing ample opportunity to discuss these theories.

REFERENCES

Baines, P.G., 1983. A survey of blocking mechanisms, with application to the Australian region. Aust. Meteorol. Mag., 31: 27–36.

Batchelor, G.K., 1953. The conditions for dynamical similarity of motions of a frictionless perfect-gas atmosphere. Q. J. R. Meteorol. Soc., 79: 224–235.

Batchelor, G.K., 1967. An Introduction to Fluid Dynamics. Cambridge University Press, London, 615 pp.

Deem, G.S. and Zabusky, N.J., 1978. Vortex waves: stationary V-states, interactions, recurrence and breaking. Phys. Rev. Lett., 40: 859–862.

Dole, R., 1982. Persistent Anomalies of the Extratropical Northern Hemisphere Wintertime Circulation. Ph.D. thesis, Department of Meteorology and Physical Oceanography, M.I.T.

Firing, E. and Beardsley, R.C., 1976. The behavior of a barotropic eddy on the beta plane. J. Phys. Oceanogr., 6: 57–65.

Flierl, G.R., 1979. Baroclinic solitary waves with radial symmetry. Dyn. Atmos. Oceans, 3: 15–38.

Flierl, G.R., 1983. The structure and motion of warm core rings. Aust. J. Mar. Freshwater Res., in press.

Flierl, G.R., Larichev, V.D., McWilliams, J.C. and Reznik, G.M., 1980. The dynamics of baroclinic and barotropic solitary eddies. Dyn. Atmos. Oceans, 5: 1–41.

Frederiksen, J.S., 1982. A unified three-dimensional instability theory of the onset of blocking and cyclogenesis. J. Atmos. Sci., 39: 969–982.

Griffiths, R.W. and Linden, P.F., 1981. The stability of vortices in a rotating stratified fluid. J. Fluid Mech., 105: 283–316.

Ingersoll, A.P. and Cuong, P.G., 1981. Numerical model of long-lived Jovian vortices. J. Atmos. Sci., 38: 2067–2076.

Larichev, V.D. and Reznik, G.M., 1976a. Two-dimensional Rossby soliton: an exact solution. Rep. U.S.S.R. Acad. Sci., 231(5): 1077–1079.

Larichev, V.D. and Reznik, G.M., 1976b. Strongly nonlinear two-dimensional isolated Rossby waves. Oceanologia, 16: 547–550.

Maxworthy, T. and Redekopp, L.G., 1976. A solitary wave theory of the Great Red Spot and other observed features in the Jovian atmosphere. Icarus, 29: 261–271.

McWilliams, J.C., Brown, E.D., Bryden, H.L., Ebbesmeyer, C.C., Elliot, B.A., Heinmiller, R.H., Lien Hua, B., Leaman, K.D., Lindstrom, E.J., Luyten, J.R., McDowell, S.C., Owens, W.B., Perkins, H., Price, J.F., Regier, L., Riser, S.C., Rossby, H.T., Sanford, T.B., Shen, C.Y., Taft, B.A. and Van Leer, J.C., 1983. The local dynamics of eddies in the western North Atlantic. In: A.R. Robinson (Editor), Eddies in Marine Science.

Nof, D., 1981. On the beta-induced movements of isolated baroclinic eddies. J. Phys. Oceanogr., 11: 1662–1672.

Ogura, Y. and Phillips, N.A., 1962. Scale analysis of deep and shallow convection in the atmosphere. J. Atmos. Sci., 19: 173–179.

Redekopp, L.G., 1977. On the theory of solitary Rossby waves. J. Fluid Mech., 82 (4): 725–745.

Rizzoli, P.M. and Hendershott, M.C., 1980. Solitary Rossby waves over variable relief and their stability. Part I: the analytical theory. Dyn. Atmos. Oceans, 4: 247–260.

Stern, M.E., 1975. Minimal properties of planetary eddies. J. Mar. Res., 33: 1–13.

The Ring Group, 1981. Gulf Stream cold-core rings: their physics, chemistry, and biology. Science, 212(4499): 1091–1100.